approaches a constant maximum value for tapers longer than 15 mm.

CONCLUSION

Planar transmission-line impedance transformers with an unconventional multilayered structure obtained by deposition of high-dielectric-constant thin films on bulk substrates have been designed and their performance have been compared to those of transformers printed on very high-dielectric-constant ($\varepsilon_r = 80$) bulk substrates. The propagation characteristics of the tapered lines were investigated using the finite-element method through a commercially available software package. The dispersion effects and impedance variation with respect to frequency were taken into account in the analysis. The response of the proposed structure does not deteriorate significantly with frequency, thus allowing operation in an acceptable range up to 40 GHz. The investigation of the propagation characteristics of short electrical pulses on the unconventional multilayered structure and on very high-dielectric-constant bulk-substrate tapers was carried out, confirming the better performance of the proposed structure. The propagation of very short pulses without substantial distortion was verified. Finally, the effects of the multilayered taper length on the performance were assessed.

The newly proposed multilayered structure presented attractive results. The achieved effective dielectric constant is very high, whereas the structure has very low dispersion, thus allowing the construction of compact high-frequency devices. The lines have both simple cross sections and comfortable transversal dimensions for a wide range of impedances, thus leading to less expensive manufacture. The results obtained thus far indicate that this structure may be suitable for many other applications in microwave components.

ACKNOWLEDGMENT

This work was supported by the Research and Development Center, Ericsson Telecomunicações S.A., Brazil.

REFERENCES

1. M.C.R. Carvalho, W. Margulis, and J.R. Souza, A new, small-sized transmission-line impedance transformer with applications in high-speed optoelectronics, IEEE Microwave Guided Wave Lett 2 (1992), 428–430.
2. M.C.R. Carvalho and L.F.M. Conrado, Ultra-short-pulse propagation in arbitrarily terminated tapered planar lines for optoelectronics applications, Microwave Opt Technol Lett 22 (1999), 85–87.
3. D.L.A. Seixas, L.F.M. Conrado, and M.C.R. Carvalho, Theoretical investigations on the propagation characteristics of transmission lines on substrates with very high dielectric constant, Microwave Opt Technol Lett 32 (2002), 275–278.
4. B. Noren, Thin-film barium strontium titanate (BST) for a new class of tunable RF components, Microwave J 47 (2004), 210–220.
5. A. Tombak, J.P. Maria, F.T. Ayguavives, Z. Jin, G.T. Stauf, A.I. Kingon, and A. Mortazawi, Voltage-controlled RF filters employing thin-film barium-strontium-titanate tunable capacitors, IEEE Trans Microwave Theory Tech 51 (2003), 462–467.
6. C. Weil, P. Wrang, H. Downar, J. Wenger, and R. Jakoby, Tunable coplanar waveguide phase shifters using ferroelectric thick films, Institut fur Hochfrequenztechnik-TUD (2002), 83–88.
7. N. Fukushima, K. Abe, M. Izuha, et al. Epitaxial (Ba,Sr)TiO_3 Capacitors with extremely high dielectric constant for DRAM applications, IEEE-IEDM 97 (1997), 257–260.
8. A.T. Findikoglu, Q.X. Jia, I.H. Campbell, X.D. Wu, D. Reagor, C.B. Mombourquette, and D. McMurry, Electrically tunable coplanar transmission line resonators using $YBa_2Cu_3O_{7-x}/SrTiO_3$ bilayers, Applied Phys Lett 66 (1995), 3674–3676.
9. D. Kuylenstierna, G. Subramanyam, A. Vorobiev, and S. Gevorgian, Tunable electromagnetic bandgap performance of CPW periodically loaded by ferroelectric varactors, Microwave Opt Technol Lett 39 (2003), 81–86.
10. S.S. Gevorgian and E.L. Kollberg, Do we really need ferroelectrics in paraelectric phase only in electrically controlled microwave devices?, IEEE Trans Microwave Theory Tech 49 (2001), 2117–2124.
11. M. Tanabe, M. Nishitsuji, Y. Anda, and Y. Ota, A low-impedance coplanar waveguide using an $SrTiO_3$ thin film for GaAs power MMIC's, IEEE Trans Microwave Theory Tech 48 (2000), 873–874.
12. M.C.R. Carvalho, L.F.M. Conrado, L.S. Demenicis, and D.L.A. Seixas, Propagation characteristics of transmission line transformers with different impedance variation patterns on substrates with very high dielectric constant, Microwave Opt Technol Lett 37 (2003), 174–177.
13. Agilent 85180A high frequency structure simulator, Ver. 5.6, September 2000.
14. R.E. Collin, Foundations for microwave engineering, 2nd ed., McGraw Hill, New York, 1992.

EXTENSION OF FORWARD-BACKWARD METHOD WITH DFT-BASED ACCELERATION ALGORITHM FOR THE EFFICIENT ANALYSIS OF LARGE PERIODIC ARRAYS WITH ARBITRARY BOUNDARIES

Özlem Aydin Civi,[1] Vakur B. Ertürk,[2] and Hsi-Tseng Chou[3]

[1] Department of Electrical and Electronics Engineering
Middle East Technical University
TR-06531, Ankara, Turkey

[2] Department of Electrical and Electronics Engineering
Bilkent University
TR-06800, Bilkent, Ankara, Turkey

[3] Department of Communications Engineering
Yuan Ze University
135 Yuan-Tung Rd.
Chung-Li 320, Taiwan

Received 24 April 2005

ABSTRACT: *An extension of the discrete Fourier transform (DFT)-based forward-backward algorithm is developed using the virtual-element approach to provide a fast and accurate analysis of electromagnetic radiation/scattering from electrically large, planar, periodic, finite (phased) arrays with arbitrary boundaries. Both the computational complexity and storage requirements of this approach are $O(N_{tot})$ (N_{tot} is the total number of unknowns). The numerical results for both printed and freestanding dipole arrays with circular and/or elliptical boundaries are presented to validate the efficiency and accuracy of this approach.*

 Microwave Opt Technol Lett 47: 293–298, 2005; Published online in Wiley InterScience (www.interscience.wiley.com). DOI 10.1002/mop.21150

Key words: *phased arrays; method of moments; discrete Fourier transform; iterative solvers*

1. INTRODUCTION

Several design tools and numerical techniques, in particular, the integral-equation-based method of moments (MoM) solutions [1], have been implemented in computer-aided design (CAD) packages to investigate the electromagnetic (EM) radiation/scattering from

large and finite, planar freestanding phased arrays and printed structures over grounded dielectric slabs accurately, since these structures have many military and commercial applications. However, the majority of conventional design and analysis methods, as well as the available CAD tools, suffer greatly from memory-storage requirements and computing time when the number of elements in the array increases rapidly.

In recent years, several MoM-based methods have been proposed to improve the operational count and memory-storage requirements of the conventional MoM [2–15]. Making use of stationary or nonstationary iterative schemes in the MoM solution reduces the operational count from $O(N_{tot}^3)$ (of order N_{tot}^3) to $O(N_{tot}^2)$, where N_{tot} is the total number of unknowns. The fast multipole method (FMM) [4] with an operational count $O(N_{tot}^{1.5})$ and its subsequent extensions such as multilevel FMM (MLFMM) [5] ($O(N_{tot} log\ N_{tot})$), as well as conjugate gradient-fast Fourier transform (CG-FFT) with $O(N_{tot} log\ N_{tot})$ [6] are some successful efforts. Besides, infinite array approximation [7], and hybrid approaches to reduce the total number of unknowns such as a hybrid combination of MoM with either uniform geometrical theory of diffraction (UTD) [8–10] or discrete Fourier transform (DFT) [11, 12] are useful techniques that are available in the literature.

Recently, a DFT-based acceleration algorithm [13] was used in conjunction with stationary (for example, the forward-backward method (FBM)) and nonstationary (for example, biconjugate gradient stabilized method (BiCGSTABM)) iterative MoM (IMoM) [14, 15] to reduce the computational complexity and memory storage of the IMoM solution to $O(N_{tot})$ in the analysis of electrically large, planar, periodic, rectangular, finite phased arrays of both freestanding and printed dipoles. In this approach (DFT-IMoM), contributions to every receiving element in the array are coming from two different regions: namely, the strong region formed by the nearby elements of the receiving element whose contributions are calculated in an element-by-element fashion, and the weak region formed by the rest of the array elements whose contributions are obtained from the DFT representation of the entire current distribution, in which only a few significant DFT terms are sufficient to provide accurate results.

In this paper, an extension of the DFT-IMoM approach has been developed to provide an efficient and accurate analysis of EM radiation/scattering from electrically large, planar, periodic, finite (phased) arrays with arbitrary boundaries, such as arrays with circular and/or elliptical boundaries, by introducing the virtual-element concept. These arrays become important when the host platform of the array has size and/or shape constraints. FBM is used as the iterative algorithm, and the method (DFT-FBM) has been applied to both freestanding and printed dipole arrays. Very accurate results have been obtained with a computational complexity and memory-storage requirement of $O(N_{tot})$. It should be noted that recently such arrays have been analyzed using a Floquet wave-based diffraction approach [16]. However, only the radiation-pattern results have been given in [16], as opposed to the results given in this paper where both the radiation-pattern and array-current distributions are accurately presented.

In section 2, the formulation of the DFT-IMoM (DFT-FBM) approach is briefly described and its implementation to the analysis of large, planar, periodic, finite (phased) arrays with arbitrary boundaries is given, considering both freestanding and printed dipoles. The numerical results are presented in section 3 and compared with conventional MoM-based reference solutions in order to validate the method's efficiency and accuracy. An $e^{j\omega t}$ time dependence is assumed and suppressed throughout this paper.

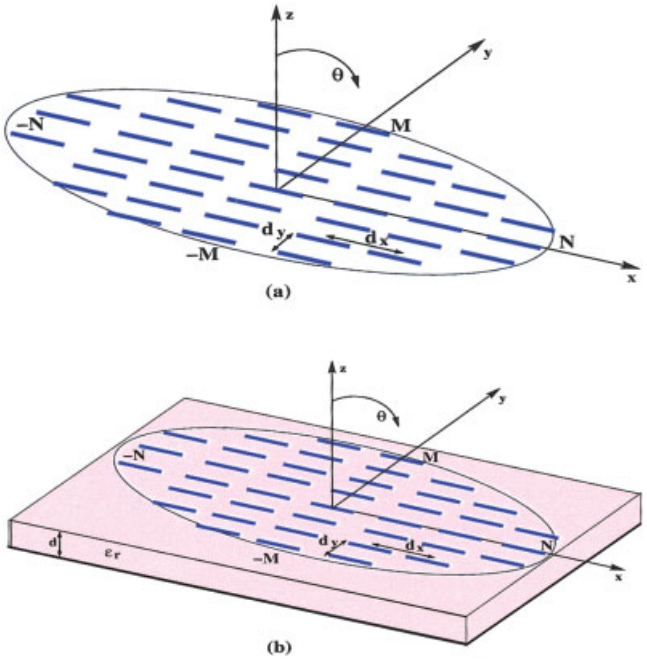

Figure 1 Geometry of a planar, irregularly contoured, periodic array of (a) freestanding and (b) printed dipoles. [Color figure can be viewed in the online issue, which is available at www.interscience.wiley.com.]

2. FORMULATION

2.1. Geometry

Consider a uniformly excited, planar, periodic array of dipoles with an arbitrary boundary. The array elements are either identical, thin, perfectly conducting wire dipoles oriented along the $\hat{x}$ direction in the $z = 0$ plane in air (freestanding dipoles), as illustrated in Figure 1(a), or identical $\hat{x}$ directed printed dipoles on a grounded dielectric slab with a thickness d and relative dielectric constant ε_r, as depicted in Figure 1(b). For both geometries, each dipole is assumed to have a length L and a width W, and to be uniformly spaced from its neighbors by distances d_x and d_y in the $\hat{x}$ and $\hat{y}$ directions, respectively. The dipoles are assumed to be center-fed with infinitesimal generators.

2.2. The Moment Method Solution

Since the array elements are thin ($W \ll L$), only $\hat{x}$-directed currents are required in the MoM modeling. Hence, the current distribution on each dipole is given by

$$J_{nm}^s(x', y') = A_{nm} f_{nm}(x', y'), \tag{1}$$

where A_{nm} is the unknown coefficient that determines the total current at the feed point on the nm^{th} ($-N \le n \le N$, $-M \le m \le M$, $(n, m) \in$ array, but the contour is not rectangular) element, and $f_{nm}(x', y')$ on the nm^{th} dipole is sinusoidal for the freestanding dipole arrays (see Fig. 1(a) and [11, 13, 15]), whereas it is piecewise sinusoidal (PWS) for the printed dipole arrays (see Fig. 1(b) and [12, 14, 15]). It should be mentioned at this point that using more than one basis function per dipole does not change the formulation but improves the accuracy.

Using an electric-field integral equation (EFIE) (formed via the boundary condition such that the total E_x vanishes on each dipole surface), and using a Galerkin MoM solution for this EFIE, a matrix equation of the form

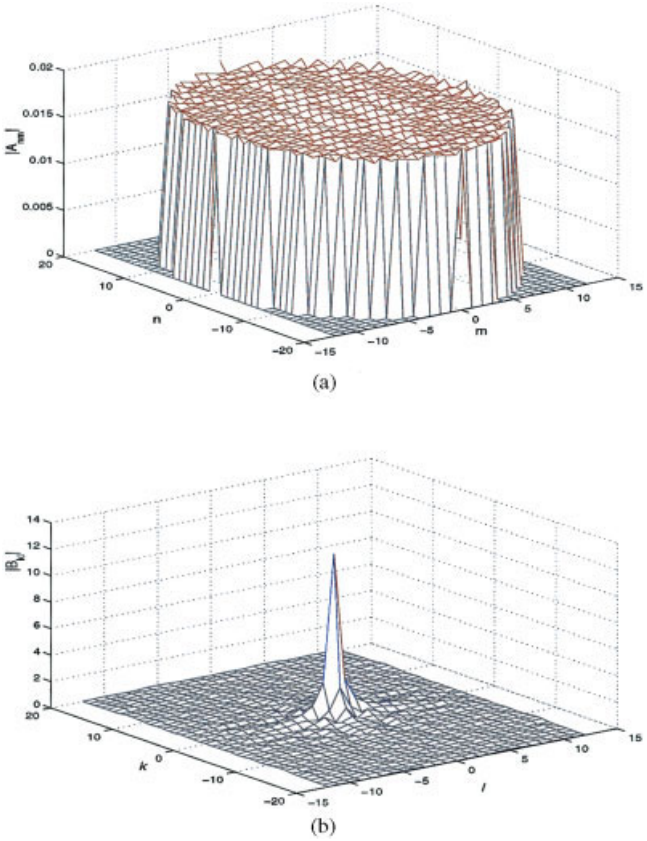

Figure 2 (a) Current amplitudes $|A_{nm}|$, and (b) DFT spectrum of the currents $|B_{kl}|$ for a uniformly excited 749-element elliptical printed dipole array. The array parameters are $(L, W) = (0.3\lambda_0, 0.01\lambda_0)$, $d_x = d_y = 0.5\lambda_0$, $\varepsilon_r = 2.55$, $d = 0.06\lambda_0$ and $(\theta, \phi) = (0°, 0°)$. [Color figure can be viewed in the online issue, which is available at www.interscience.wiley.com.]

$$\bar{\mathbf{Z}} \cdot \mathbf{I} = \mathbf{V} \tag{2}$$

is obtained. In (2), $\mathbf{I} = [A_{nm}]$ is the unknown vector of expansion coefficients and $\bar{\mathbf{Z}} = [Z_{nm,pq}]$ is the impedance matrix of the array with elements $Z_{nm,pq}$, which denotes the mutual impedance between the nm^{th} and pq^{th} $(-N \le p \le N, -M \le q \le M, (p, q) \in$ array) dipoles, given by

$$Z_{nm,pq} = \int_{S_{pq}} dS_{pq} \int_{S_{nm}} dS'_{nm} f_{pq}(\mathbf{r}_{pq}) G_{xx}(\mathbf{r}_{pq}|\mathbf{r}'_{nm}) f_{nm}(\mathbf{r}'_{nm}), \tag{3}$$

where $\mathbf{r}_{pq}$ and $\mathbf{r}'_{nm}$ are the position vectors of the pq^{th} and nm^{th} dipoles. Finally, $G_{xx}(\mathbf{r}_{pq}|\mathbf{r}'_{nm})$ is the corresponding component of the (i) free-space dyadic Green's function for the freestanding dipole array, and the (ii) planar microstrip dyadic Green's function [17] for the printed dipole array. On the other hand, $\mathbf{V}$ at the right hand side of (2) is the voltage vector related to the excitation of the pq^{th} element given by $V_{pq} e^{-jk_x p d_x} e^{-jk_y q d_y}$ with

$$k_x = k_0 \sin\theta_i \cos\phi_i; \; k_y = k_0 \sin\theta_i \sin\phi_i, \tag{4}$$

where (θ_i, ϕ_i) is the scan direction of the beam.

2.3. Review of Forward-Backward Method (FBM) for Phased Arrays

Similar to [14], the FBM is employed to solve (2) by first splitting the total current into forward and backward components, namely, $\mathbf{I} = \mathbf{I}^f + \mathbf{I}^b$, where $\mathbf{I}^f$ is the forward component denoting the current distribution due to the wave propagation in the forward direction and $\mathbf{I}^b$ is its backward correction. Hence, the matrix equation given by (2) is transformed to

$$\bar{\mathbf{Z}}^s \cdot \mathbf{I}^f = \mathbf{V} - \bar{\mathbf{Z}}^f \cdot (\mathbf{I}^f + \mathbf{I}^b); \; \bar{\mathbf{Z}}^s \cdot \mathbf{I}^b = -\bar{\mathbf{Z}}^b \cdot (\mathbf{I}^f + \mathbf{I}^b) \tag{5}$$

where $\bar{\mathbf{Z}}^s$, $\bar{\mathbf{Z}}^f$, and $\bar{\mathbf{Z}}^b$ are the diagonal, lower, and upper triangular parts of the impedance matrix $\bar{\mathbf{Z}}$, respectively. Initializing $\mathbf{I}^b$ to zero at the first iteration, (5) is solved for $\mathbf{I}^f$ and $\mathbf{I}^b$ by forward and backward substitutions, respectively. Iterations are continued until convergence is provided; this requires, in general, three or four iterations.

2.4. DFT-Based Acceleration Algorithm

The computational complexity and memory storage of FBM is $O(N_{tot}^2)$ due to the repeated and time-consuming computations of $\bar{\mathbf{Z}}^f \cdot \mathbf{I}$ and $\bar{\mathbf{Z}}^b \cdot \mathbf{I}$, which prohibits its application to very large arrays. Therefore, the DFT-based acceleration algorithm is used in conjunction with FBM, which is based on using the DFT spectrum of currents to reduce computational complexity. As shown in Figure 2(a), a typical current distribution on array elements is quite different from the feed distribution, especially near the array boundary. Hence, to find the current distribution on the array and the input impedances of the elements accurately, one has to analyze the complete array using rigorous numerical methods. However, the DFT spectrum of practical array currents are very compact, as seen in Figure 2(b). Consequently, the selection of a few significant DFT terms from the DFT spectrum is sufficient to provide accurate results. These significant DFT terms are selected based on the criteria given in [11].

The DFT-based acceleration algorithm is actually well-suited for the fast and accurate analysis of rectangular arrays (freestanding and printed) [13–15]. Therefore, to implement this algorithm efficiently, the arrays shown in Figure 1 are mathematically extended into a rectangular array with virtual elements as shown in Figure 3. All the virtual elements are located external to the array

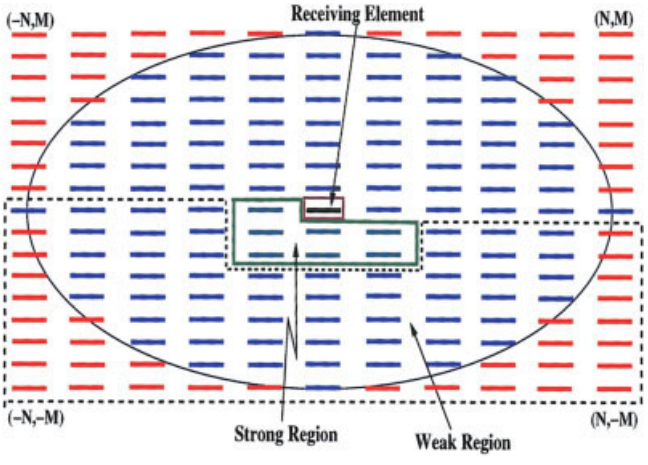

Figure 3 In the extended array, decomposition of interaction elements in terms of strong and weak groups with respect to the pq^{th} receiving element. The virtual elements are the dipoles (marked with red) located external to the array boundary. [Color figure can be viewed in the online issue, which is available at www.interscience.wiley.com.]

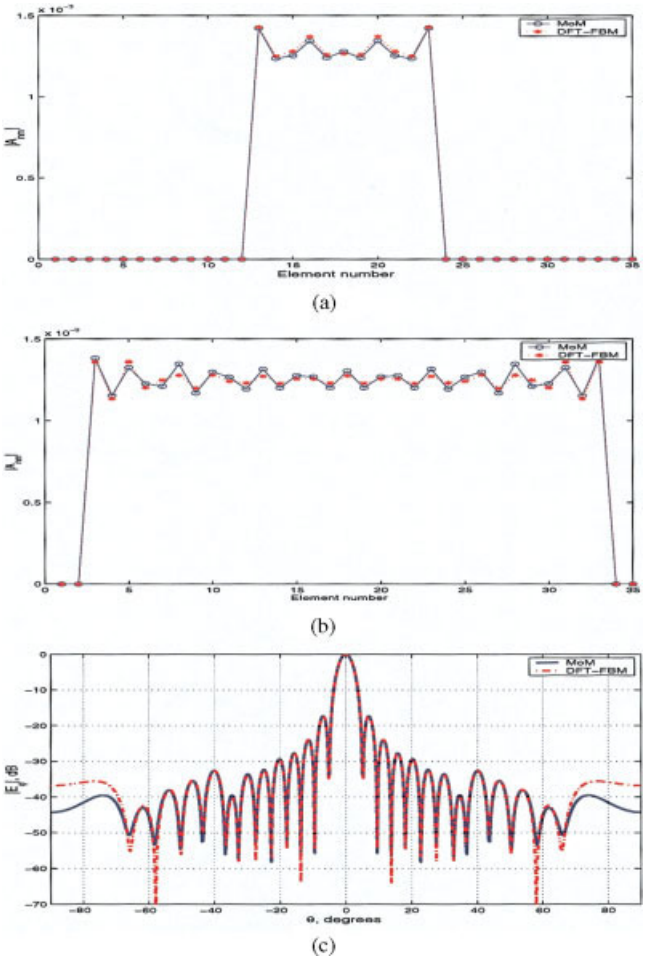

Figure 4 Comparison of the magnitude of induced current $|A_{nm}|$ for the (a) 2nd row and (b) 11th rows and (c) the radiation pattern obtained via DFT-FBM and conventional MoM of a 901-element (35 × 35) elliptical, uniformly excited freestanding dipole array. The array parameters are (L, W(radius)) = ($0.4\lambda_0$, $0.001\lambda_0$), $d_x = 0.7\lambda_0$, $d_y = 0.4\lambda_0$ and (θ, ϕ) = (0°, 0°). Size of the strong region = 5 × 5. Number of DFT terms = 3. [Color figure can be viewed in the online issue, which is available at www.interscience.wiley.com.]

boundary. Then, similar to [13–15], this DFT-based acceleration algorithm is implemented. Briefly, the contributing elements in front of the receiving element are divided into "strong" and "weak" interaction groups (Fig. 3), such that

$$[\bar{\mathbf{Z}} \cdot \mathbf{I}]_{pq} = \sum_{nm \in strong} A_{nm} Z_{nm,pq} + \sum_{nm \in weak} A_{nm} Z_{nm,pq}. \quad (6)$$

The number of elements which remain in the strong group is fixed and very small compared to the number of elements in the entire array, but contributions coming from this group assure the fundamental accuracy of the method and, hence, are obtained in an exact element-by-element fashion. On the other hand, although contributions coming from the weak group provide only minor corrections, their evaluation without the acceleration algorithm would constitute the most time-consuming aspect of the MoM calculations. Therefore, the weak region contribution to the pq^{th} receiving element, given by

$$E_{weak}(\mathbf{r}_{pq}) = \sum_{nm \in weak} A_{nm} Z_{nm,pq}, \quad (7)$$

is rewritten as

$$E_{weak}(\mathbf{r}_{pq}) = \sum_{k=-N}^{N} \sum_{l=-M}^{M} B_{kl} \sum_{nm \in weak} Z_{nm,pq} e^{-jk_x n d_x} e^{-jk_y m d_y} e^{-j2\pi(kn/2N+1)} e^{-j2\pi(lm/2M+1)} \quad (8)$$

by using the DFT expansion of the unknown coefficients A_{nm}, which is expressed as

$$A_{nm} = e^{-jk_x n d_x} e^{-jk_y m d_y} \sum_{k=-N}^{N} \sum_{l=-M}^{M} B_{kl} e^{-j2\pi(kn/2N+1)} e^{-j2\pi(lm/2M+1)}, \quad (9)$$

with B_{kl} being the coefficient of the kl^{th} DFT term. Using only the important DFT terms [due to the compactness of the DFT spectrum, as shown in Fig. 2(b)], which are a few but significant so that the accuracy is maintained, results in

$$E_{weak}(\mathbf{r}_{pq}) = \sum_{kl \in Q} B_{kl} C_{kl,pq}, \quad (10)$$

where Q denotes the selected DFT terms, and

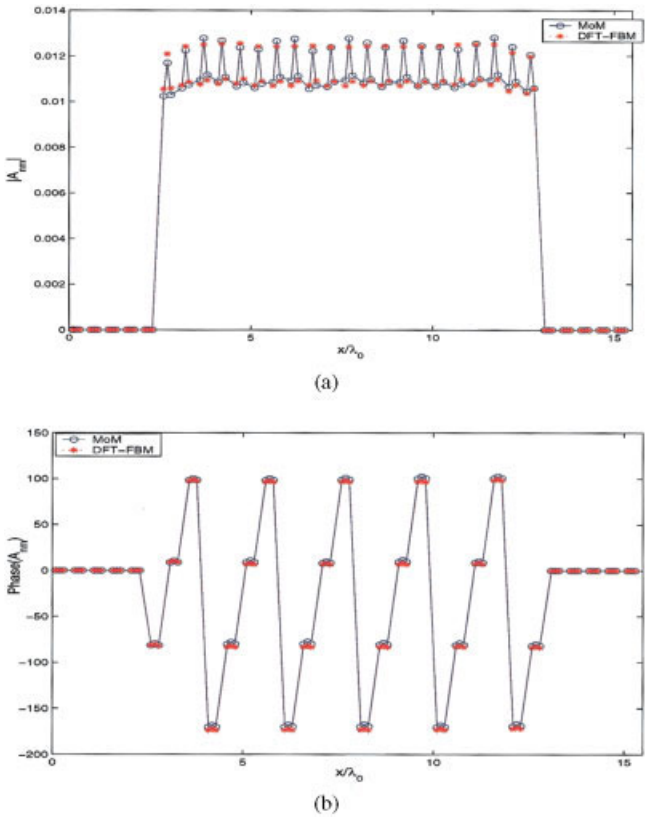

Figure 5 (a) Magnitude and (b) phase of the current amplitudes on the 5th row of a 709-element (31 × 31) circular, uniformly excited printed dipole array. The array parameters are (L, W) = ($0.39\lambda_0$, $0.01\lambda_0$), $d_x = d_y = 0.5\lambda_0$, $\varepsilon_r = 2.55$, $d = 0.06\lambda_0$ and (θ, ϕ) = (30°, 0°). Size of the strong region = 3 × 3. The number of DFT terms = 5, and three basis functions per dipole are used. [Color figure can be viewed in the online issue, which is available at www.interscience.wiley.com.]

$$C_{kl,pq} = \sum_{nm \in weak} Z_{nm,pq} e^{-jk_x nd_x} e^{-jk_y md_y} e^{-j2\pi(kn/2N+1)} e^{-j2\pi(lm/2M+1)}. \quad (11)$$

$C_{kl,pq}$ in (11) denotes the contribution of the kl^{th} DFT term to the pq^{th} receiving element and can be calculated very efficiently in an iterative fashion for the rectangularly contoured arrays, as demonstrated in [13–15].

On the other hand, the arrays we consider in this paper are irregularly contoured arrays and are extended to rectangularly contoured ones by introducing the virtual elements so that Eqs. (6)–(11) can be used. However, when using these equations, it should be assumed that currents on these elements are exactly zero (that is, $A_{nm} = 0$ for virtual elements). Therefore, in the evaluation of the strong region contributions, both the voltages on these elements and the mutual coupling between and with these elements are set to zero. In other words,

$$V_{pq} = 0 \quad \text{if } pq \in \text{virtual element}, \quad (12)$$

and

$$Z_{nm,pq} = 0 \quad \text{if } nm \text{ and/or } pq \in \text{virtual element}. \quad (13)$$

Implementation of (12) and (13) will assure that $A_{nm} = 0$ for virtual elements.

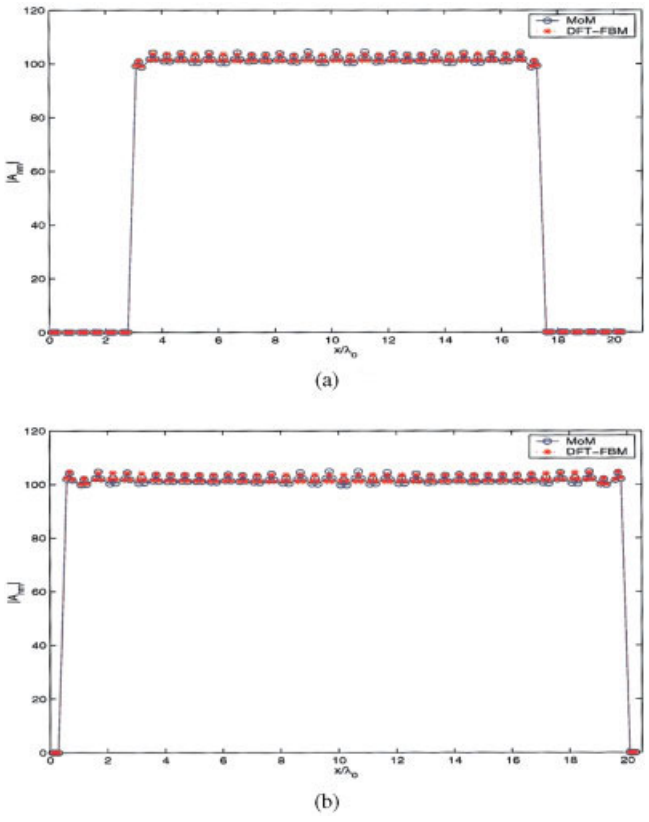

Figure 6 Comparison of the magnitude of induced current $|A_{nm}|$ for the (a) 4^{th} and (b) 11^{th} rows obtained via DFT-FBM and conventional MoM for a 749-element (41 × 25) elliptical, uniformly excited printed dipole array. The array parameters are $(L, W) = (0.39\lambda_0, 0.01\lambda_0)$, $d_x = d_y = 0.5\lambda_0$, $\varepsilon_r = 2.55$, $d = 0.06\lambda_0$ and $(\theta, \phi) = (0°, 0°)$. The size of the strong region = 3 × 3, the number of DFT terms = 5, and three basis functions per dipole are used. [Color figure can be viewed in the online issue, which is available at www.interscience.wiley.com.]

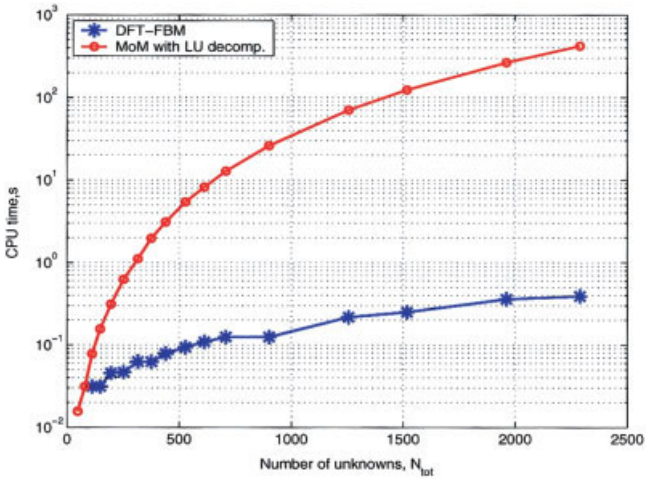

Figure 7 Comparison of CPU times for DFT-FBM and MoM with LU decomposition for printed dipole arrays. The array and the substrate parameters are the same as the ones used in Figs. 5 and 6. [Color figure can be viewed in the online issue, which is available at www.interscience.wiley.com.]

On the other hand, in the evaluation of the weak-region contributions, such as the computation of (11), each $Z_{nm,pq}$ between a virtual element and a real element, as well as each $Z_{nm,pq}$ between two virtual elements, are identical to those between real elements (that is, they are now nonzero as opposed to (13)). Since the A_{nm} values of virtual elements are now taken as zero in the computation of the B_{kl} values, utilization of nonzero $Z_{nm,pq}$ values will not cause any problem if all DFT terms are employed. In reality, insignificant errors might occur due to the use of few DFT terms. However, that amount of error in the computation of contributions coming from the weak region will not affect the overall accuracy.

3. NUMERICAL RESULTS

To assess the accuracy and efficiency of this proposed approach for the analysis of irregularly contoured arrays, numerical results pertaining to both freestanding and printed dipole arrays are obtained and compared with the results obtained via conventional MoM. In all examples, the arrays are excited uniformly in amplitude so that $V_{pq} = 1$ in (2) for each pq^{th} dipole.

In Figures 4(a) and 4(b), current amplitudes $|A_{nm}|$ versus the element position on the 2^{nd} and 11^{th} rows are evaluated using DFT-FBM and compared with the conventional MoM solution pertaining to a 901-element elliptical (the size of the corresponding rectangular array after introducing the virtual elements is 35 × 35), uniformly excited freestanding dipole array with $d_x = 0.7\lambda_0$ and $d_y = 0.4\lambda_0$ (with λ_0 being the free-space wavelength). The length and radius of each dipole are $0.4\lambda_0$ and $0.001\lambda_0$, respectively. The elements are phased to radiate a beam in broadside direction, as shown in Figure 4(c). As seen from the figure, very good agreement is obtained using just three DFT coefficients and 5 × 5 strong regions (12 elements in forward and 12 elements in backward runs). Less than 2% error is achieved with just three iterations, and the elapsed CPU time for DFT-FBM is 0.17 sec, whereas it is 10.4 sec for the conventional MoM approach.

Figures 5(a) and 5(b) depict the magnitude and phase of current amplitudes versus element position on the 5^{th} row of a 709-element circular (the size of the corresponding rectangular array after introducing the virtual elements is 31 × 31), uniformly excited printed dipole array on a $0.06\lambda_0$ thick substrate with $\varepsilon_r = 2.55$. Each dipole has a dimensions of $(L, W) = (0.39\lambda_0,$

$0.01\lambda_0$) and they are spaced from each other by distances $d_x = d_y = 0.5\lambda_0$ in the $\hat{x}$ and $\hat{y}$ directions, respectively. The elements are phased to radiate a beam in the $(\theta, \phi) = (30°, 0°)$. For this example, the size of the strong region is 3×3 (four elements in forward and four elements in backward runs), and five DFT terms are used. Again a residual error less than 1.5% error is achieved with three iterations. The elapsed CPU time for DFT-FBM is 0.625 sec for this example. Using a conventional MoM approach requires a CPU time of 595.9 sec. Note that three basis functions per dipole is used for this example.

As a third example, a 749-element printed dipole with an elliptical boundary is considered (the size of the corresponding rectangular array after introducing the virtual elements is 41×25). The array and the substrate parameters are the same as the previous example. Figures 6(a) and 6(b) show a comparison of the magnitude of induced current $|A_{nm}|$ for the 4^{th} and 11^{th} rows, respectively, obtained via DFT-FBM and conventional MoM. The size of the strong region, the number of DFT terms, and the residual error are also the same as the previous example.

As seen in all examples, very good agreement between the DFT-FBM and conventional MoM results has been achieved, thereby establishing confidence in the present DFT-FBM approach. Finally, the CPU times of the DFT-FBM approach and MoM with LU decomposition is compared in Figure 7 for a printed dipole array whose parameters are the same as the ones used in the aforementioned numerical results. As illustrated in the figure, the required CPU time for the DFT-FBM approach is very small compared to that required in the conventional MoM, especially when N_{tot} is very large.

4. DISCUSSIONS AND CONCLUSIONS

Efficient and accurate analysis of electrically large, planar, periodic, finite (phased), arbitrarily contoured arrays of both freestanding and printed dipoles has been presented by introducing the virtual-element concept. Both the computational complexity and the memory-storage requirements are $O(N_{tot})$. The efficiency and accuracy of the method have been demonstrated by numerical results in the form of current distributions on and far-field radiation patterns of various arrays with irregular contours.

REFERENCES

1. R.F. Harrington, Field computation by moment methods, IEEE Press, Piscataway, NJ, 1993.
2. A. Ishimaru, R.J. Coe, G.E. Miller, and V.P. Green, Finite periodic approach to large scanning array problems, IEEE Trans Antennas Propagat 31 (1985), 54–59.
3. H.-T. Chou, Extension of the forward-backward method using spectral acceleration for the fast analysis of large array problems, IEE Proc Microwave Antennas Propagat 147 (2000), 167–172.
4. N. Engheta, W.D. Murphy, V. Rokhlin, and M.S. Vassiliou, The fast multipole method (FMM) for electromagnetic scattering problems, IEEE Trans Antennas Propagat 40 (1992), 634–641.
5. X.Q. Sheng, J.-M. Jin, J. Song, W.C. Chew, and C.-C. Lu, Solution of combined-field integral equation using multilevel fast multipole algorithm for scattering by homogeneous bodies, IEEE Trans Antennas Propagat 46 (1998), 1718–1726.
6. Y. Zhuang, K.-L. Wu, C. Wu, and J. Litva, A combined full-wave CG-FFT method for rigorous analysis of large microstrip antenna arrays, IEEE Trans Antennas Propagat 44 (1996), 102–109.
7. A.K. Skrivervik and J.R. Mosig, Finite phased array of microstrip patch antennas: the infinite array approach, IEEE Trans Antennas Propagat 40 (1992), 579–582.
8. Ö.A. Civi, P.H. Pathak, H.-T. Chou, and P. Nepa, A hybrid uniform geometrical theory of diffraction-moment method for the efficient analysis of electromagnetic radiation/scattering from large finite planar arrays, Radio Science 35 (2000), 607–620.
9. A. Neto, S. Maci, G. Vecchi, and M. Sabbadini, A truncated Floquet wave diffraction method for the full-wave analysis of large phased arrays, part 2: generalization to 3D cases, IEEE Trans Antennas Propagat 48 (2000), 601–611.
10. Ö.A. Civi, V.B. Ertürk, P.H. Pathak, P. Janpugdee, and H.-T. Chou, A hybrid UTD-MoM approach for the efficient analysis of radiation/scattering from large, printed finite phased arrays, 2001 IEEE AP-S International Symposium and USNC/URSI Meeting, Boston, MA, 806–809.
11. H.-T. Chou, H.-K. Ho, P.H. Pathak, P. Nepa, and Ö.A. Civi, Efficient hybrid discrete Fourier transform-moment method for fast analysis of large rectangular arrays, IEE Proc Microwave Antennas Propagat 149 (2002), 1–6.
12. H.-T. Chou, H.-K. Ho, Ö.A. Civi, and V.B. Ertürk, Applications of hybrid discrete Fourier transform-moment method to the fast analysis of large rectangular dipole arrays printed on a thin grounded dielectric substrate, Microwave Opt Technol Lett 34 (2002), 203–207.
13. H.-T. Chou and H.-K. Ho, Implementation of a forward-backward procedure for the fast analysis of electromagnetic radiation/scattering from two-dimensional large phased arrays, IEEE Trans Antennas Propagat 52 (2004), 388–396.
14. Ö.A. Civi, Extension of forward backward method with DFT based acceleration algorithm for the efficient analysis of radiation/scattering from large finite printed dipole arrays, Microwave Opt Technol Lett 37 (2003), 20–26.
15. V.B. Ertürk and H.-T. Chou, Efficient analysis of large phased arrays using iterative MoM with DFT based acceleration algorithm, Microwave Opt Technol Lett 39 (2003), 89–94.
16. E. Martini, A. Toccafondi, S. Maci, and R. Tiberio, Floquet wave-based diffraction approach for irregularly contoured planar phased arrays, IEEE Antennas and Wireless Propagat Letters 2 (2003), 246–249.
17. S. Barkeshli, P.H. Pathak, and M. Marin, An asymptotic closed-form microstrip surface Green's function for the efficient moment method analysis of mutual coupling in microstrip antennas, IEEE Trans Antennas Propagat 38 (1990), 1374–1383.

BROADBAND DUAL-POLARIZED PROXIMITY COUPLED CIRCULAR PATCH ANTENNA

S. Gao and A. Sambell
School of Engineering and Technology
Northumbria University
Newcastle Upon Tyne, Northern 8ST, United Kingdom

Received 20 April 2005

ABSTRACT: *This paper presents the design and results of a novel broadband dual-polarized circular patch antenna. The antenna is fed by microstrip lines through proximity coupling, and H-shaped slots are cut in the ground plane below the feed lines for enhancing the coupling between the patch and the feed lines. By using only a single circular microstrip patch, the prototype antenna yields bandwidth of 21.5% and 25.9% at the input ports 1 and 2, respectively. The isolation between two input ports is below −30 dB across the bandwidth. Good broadside radiation patterns are observed, and the cross-polar levels are below −20 dB at both* E- *and* H-*planes. Due to its simple structure, it is easy to form arrays by using this antenna as an element.* © 2005 Wiley Periodicals, Inc. Microwave Opt Technol Lett 47: 298–302, 2005;
Published online in Wiley InterScience (www.interscience.wiley.com).
DOI 10.1002/mop.21151